Particuology 56 (2021) 183–192

Contents lists available at ScienceDirect

Particuology

journal homepage: www.elsevier.com/locate/partic

Mesoscale analysis of the suction stress characteristic curve for unsaturated granular materials

Xiaoliang Wang[a,*], Zhen Zhang[b], Jiachun Li[b,c,**], Qingquan Liu[a]

[a] Department of Mechanics, School of Aerospace Engineering, Beijing Institute of Technology, Beijing 100081, China
[b] Key Laboratory for Mechanics in Fluid Solid Coupling Systems, Institute of Mechanics, Chinese Academy of Sciences, Beijing 100190, China
[c] School of Engineering Science, University of Chinese Academy of Sciences, Beijing 100049, China

ARTICLE INFO

Article history:
Received 15 November 2019
Received in revised form 8 September 2020
Accepted 25 September 2020
Available online 2 November 2020

Keywords:
Suction stress
Liquid bridge
Unsaturated granular material
Discrete element method

ABSTRACT

There is still no theoretical framework accounting for linkage between seepage and deformation of unsaturated granular materials. Using a mesoscale liquid bridge model, we propose the first approach for deriving the suction stress characteristic curve (SSCC). Then, we verify the method by obtaining both the soil–water characteristic curve and SSCC for cubic and tetrahedral granular packing. The approach is further validated by generating the SSCCs of granular packings with different particle size distributions. On this basis, a new two-parameter model is suggested that satisfactorily predicts the SSCCs of various real granular materials. The nonlinear variation of strength versus suction is also properly described by a new formula for three kinds of soil. We believe that this SSCC model can help resolve solid–fluid coupling in seepage and deformation problems in unsaturated granular engineering.

Introduction

Presently, the surface of the earth is widely covered with arid and semi-arid areas from latitude 10° to 40°, where rainfall is less than evaporation (Fredlund, Rahardjo, & Rahardjo, 1993). The thickness of an unsaturated granular material layer such as loess or expansive soil always exceeds tens of meters or is even more than 100 m. Therefore, unsaturated soil mechanics is very significant especially to local inhabitants when dealing with such issues as infrastructure, residence safety, agricultural hydrology and geological disasters. People began to have a deeper understanding of foundation capacity, earth wall strength and slope stability when geotechnical engineering became well developed. In that period, Karl Terzaghi summarized three main kinds of problems: seepage, deformation and strength for geomaterial and geomechanics.

Soil mechanics of saturated granular materials has been well established on the basis of Terzaghi's effective stress theory (Terzaghi, 1925), which is now termed Biot theory (Biot, 1941). In contrast, the theoretical framework for unsaturated granular materials is still pending. For a seepage problem, two constitutive laws known as the soil–water characteristic curve (SWCC) and hydraulic conductivity function (HCF) are well formulated to derive a parabolic governing equation system (Lu & Likos, 2004).

Several researchers have developed the general effective stress and two-variable frameworks for coupling of seepage and deformation in unsaturated granular materials. Bishop (1959) first proposed an effective stress model linking both total net stress and suction with one parameter χ, which is derived by numerical fitting based on experimental data for real soils from case to case. Moreover, because χ has no obvious physical meaning, the results obtained this way may lead to a poor mathematical expression which only fits for one kind of granular material. The situation limits the application of Bishop's effective stress model. As for the two-variable framework of net stress and suction, several important constitutive models such as the Barcelona basic model (BBM) (Alonso, Gens, & Josa, 1990) have been presented. However, a series of parallel experiments including hydraulic behavior, structural deformation and their coupling are required for identifying parameters in the BBM, which greatly limits on-site usage.

Regarding strength theory for unsaturated granular materials such as compact glacial till (Gan, Fredlund, & Rahardjo, 1988) and red silt (Escario, 1989), the nonlinear variation of strength versus suction should be accounted for. One widely used strength theory for unsaturated granular materials is extended Mohr–Coulomb

* Corresponding author.
** Corresponding author at: Key Laboratory for Mechanics in Fluid Solid Coupling Systems, Institute of Mechanics, Chinese Academy of Sciences, Beijing 100190, China.
E-mail addresses: wangxiaoliang36@bit.edu.cn (X. Wang), jcli05@imech.ac.cn (J. Li).

https://doi.org/10.1016/j.partic.2020.09.008

theory, which includes the suction as an additional term with a constant coefficient $\tan\phi^b$. The model is in fact a reformulation of Bishop's effective stress concept (Lu & Likos, 2004). The difficulty of the nonlinear behavior of strength versus suction has not been fully resolved by extended Mohr–Coulomb theory. Even if the empirical constant $\tan\phi^b$ is treated as variable, numerically fitted results are usually unsatisfactory and vary from case to case.

In 2006, Lu and Likos (2006) proposed an innovative concept of suction stress in an abstract representative volume element of an air–water–particle system. Then, a new constitutive description known as a suction stress characteristic curve (SSCC) was developed. Later, Lu answered the question "Is matric suction a stress variable" in an in-depth study of an unsaturated porous medium (Lu, 2008). He claimed that matric suction is a stress state variable rather than a stress variable. However, if matric suction is used in a constitutive model, the strong interdependency between matric suction and net stress should be suitably clarified. This is the main reason why Bishop's effective stress model and extended Mohr–Coulomb theory fail to model unsaturated granular materials. As for the SSCC, Lu, Godt, and Wu (2010) formulated a closed form from the thermodynamics of an air–water–particle system, but with surface tension neglected in pendular and funicular regimes. Many real soil samples were used to validate Lu's SSCC model for cases in the capillary regime. Furthermore, if the parameter χ is chosen at saturation, the model recovers Bishop's effective stress theory, which has already been verified within limit. Lu's suction stress and SSCC theory have made considerable progress in dealing with effective stress in unsaturated granular materials.

The discrete element method (DEM) (Cundall & Strack, 1979) starting from particle interaction and dynamics provides another way to handle mechanics of granular materials from a mesoscale or even microscale viewpoint. Recent DEM advances include calculating mechanical behavior such as strength/dilatancy for dry granular materials (Belheine, Plasslard, Donze, Darve, & Seridi, 2009; Wang & Li, 2014; Wang, Zhang, & Li, 2019). There are also important achievements in modeling unsaturated granular materials with the liquid bridge model (Scholtès, Chareyre, Nicot, & Darve, 2009; Wang & Li, 2015a) and pore network fluid flow model (Caulk, Sholtès, Krzaczek, & Chareyre, 2020; Yuan & Chareyre, 2017). Therefore, as to the SSCC, we ask the questions: Can we produce suction stress and an SSCC using mesoscale liquid bridge or Young–Laplace theory (Scholtès et al., 2009; Wang & Li, 2015a)? Is there an SSCC model that can be applied in the whole range of capillary, funicular and pendular regimes?

The objective of this study is to answer these questions. This paper is organized as follows. Section 2 briefly reviews the DEM and the liquid bridge model, and addresses the definition of suction stress with two examples for verification. On the basis of the liquid bridge model and DEM simulation, section 3 derives the SSCCs of two parallel series of particle packings with dispersive particle size distributions (PSDs). Next, we work out a new SSCC model and compare it with DEM simulations together with several experiments on real soils. Then the new SSCC model is used to examine the nonlinear variation of strength with suction for unsaturated granular materials. In the end, we summarize the major findings of this study.

Liquid bridge model and its verification

This section briefly reviews the liquid bridge model presented in our previous paper (Wang & Li, 2015a) and basic computational procedures in the DEM. Two additional examples are provided for further model verification.

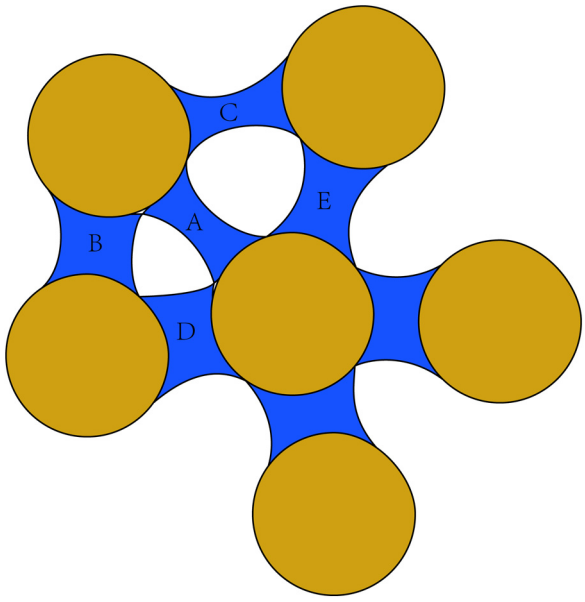

Fig. 1. 2D sketch of a liquid bridge–particle system of real 3D packing. Brown circles denote particles; the blue meniscus represents a liquid bridge.

Liquid bridge model

Adding some water into a granular system makes a cohesive material owing to the capillary effect. The original liquid bridge model is used to calculate the cohesive force between particles and the water volume via the Young–Laplace theory (Scholtès et al., 2009). However, Young–Laplace theory is only suitable for low water content in a pendular regime. The modified liquid bridge model is used to compute cohesive force and water volume for high water content such as in funicular and capillary regimes (Wang & Li, 2015a). The air volume is redistributed as the liquid bridge force is reduced in the funicular and capillary regimes:

$$V_a^i = \left(V_V - \sum_j V_m^j\right) \cdot \frac{m_i}{\mathrm{Max}Me}, \tag{1}$$

$$F_{cap}^{'} = F^{cap} \cdot \frac{1}{(1+m_i)}, \tag{2}$$

where V_a^i is the volume of water added to the ith liquid bridge if fusion occurs, V_V is the total volume of pores, V_m^j denotes the volume of the jth liquid bridge in Young–Laplace theory, $F_{cap}^{'}$ is the bridge force, F^{cap} is the original bridge force, and m_i is the fusion number of the ith bridge, which is equal to the number of bridges that contact or overlap with the ith bridge. MaxMe indicates the average maximal fusion number, which is easily obtained through its value in the saturated regime.

Fig. 1 shows a two-dimensional sketch for a real three-dimensional case. Liquid bridge A overlaps with four liquid bridges B, C, D and E, so the fusion number m_i of bridge A is 4. The liquid bridge force $F_{cap}^{'}$ decreases linearly with the fusion number from the original liquid bridge force F^{cap} in Young–Laplace theory (Scholtès et al., 2009; Wang & Li, 2015a). If there is no fusion as in the pendular regime, then m_i is zero, and the modified method recovers the original Young–Laplace theory (Cundall & Strack, 1979). We also define two microscopic indicators, the average number of liquid bridges per particle, Ke, and average fusion number per liquid bridge, Me, to characterize the unsaturated granular system.

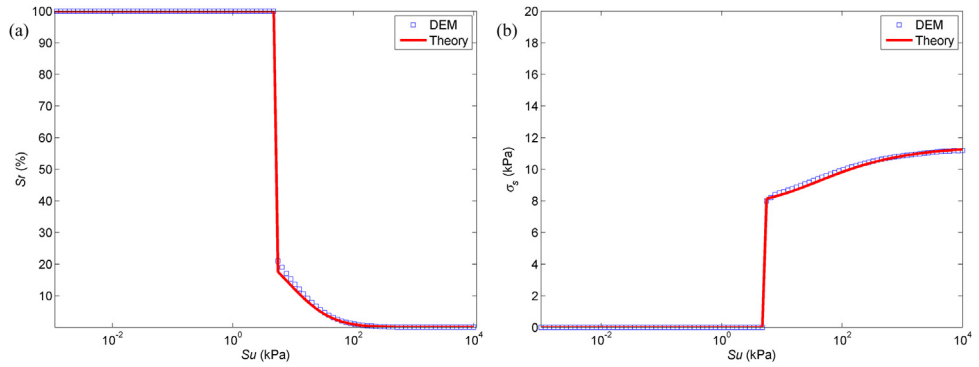

Fig. 2. SWCC (a) and SSCC (b) of cubic granular packing with a diameter of 0.02 mm, where *Sr* is saturation and *Su* is suction.

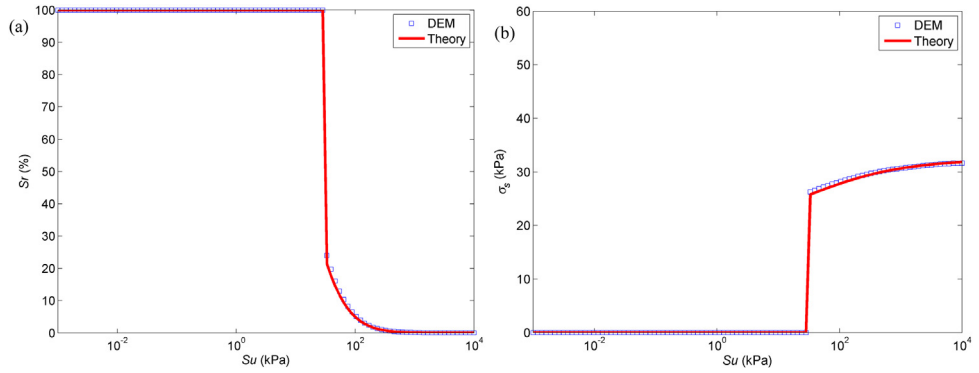

Fig. 3. SWCC (a) and SSCC (b) of tetrahedral granular packing with a diameter of 0.02 mm, where *Sr* is saturation and *Su* is suction.

Suction stress

Lu and Likos (2006) regarded suction stress as an abstract concept that actually represents the tension due to matric suction. Lu (2008) also claimed that suction is not a state variable, which causes many difficulties in Bishop's effective stress framework. The decomposition of total net stress $\sigma - u_a$ (where σ is total stress and u_a is air pressure) into effective stress σ' and suction stress σ_s is

$$\sigma - u_a = \sigma' + \sigma_s. \tag{3}$$

In the liquid bridge model, suction stress is computed as an average contribution of liquid bridge force:

$$\sigma_s = \frac{1}{3} trace[\frac{1}{V}\sum F_{ij}^{cap'} l_{ij}], \tag{4}$$

where l_{ij} is the branch vector from the center of the ith particle to that of the jth particle.

The suction stress of a material can be regarded as a state variable like pressure, while suction is only an external load. The relationship between suction stress σ_s and suction *Su* is termed the suction stress characteristic curve (SSCC) (Lu & Likos, 2006).

Computational procedure

It is optional whether to specify the suction or water volume first. In this study, we implemented the above liquid bridge model into a DEM code to develop a suction control engine for unsaturated granular materials (Wang & Li, 2015a). The contact force is calculated via the classical interaction model, and the liquid bridge model accounts for the hydraulic component between particles. First, we model a granular sample by generating granular packing of more than 10,000 spherical particles with more than 20 particles along each dimension with a specified PSD. Stress loading is applied to compress the granular system to a specified isotropic stress state. Then, adjustable suction is applied externally to inspect the hydraulic and stress processes. As soon as external suction is exerted on generated samples, we start to observe and record the hydraulic response including water content, suction stress and microscopic indicators such as liquid bridge number, coordination number and fusion number.

Contact force includes normal and tangential contact forces via the linear spring model. The normal stiffness k_n and tangential stiffness k_s are calculated in the Yade formulation (Wang & Li, 2014) as $k_n = 2\frac{ER_1R_2}{R_1+R_2}$ and $k_s = \alpha k_n$ for a contacting pair with radii R_1 and R_2, where E is Young's modulus and α is Poisson's ratio. A Coulomb friction law is applied to estimate the tangential force limit using a friction coefficient $\mu = \tan(\phi_p)$, where ϕ_p is the friction angle between particles. These mechanical contact laws primarily govern the macroscopic mechanical behavior of granular materials; therefore we select the typical values $E = 50$ Mpa, $\alpha = 0.4$ and $\phi_p = 30^\circ$ in all the following simulations.

Verification

We give two examples of cubic and tetrahedral packing of particles of the same size to verify the model by comparing with theoretical solutions available for both the SWCC and SSCC (Wang & Li, 2015a). The liquid bridge model is used to calculate both the SWCC and SSCC of these two simple packings with a particle diameter of 0.02 mm. The SWCC and SSCC for cubic packing are shown in Fig. 2(a) and (b), and those of tetrahedral packing in Fig. 3(a) and (b). For high suction (low water content), the liquid bridges separate from each other. Rising water content reduces suction. The suction stress decreases also. All the pores instantly fill with water until the critical filling angle is reached, 45° for cubic packing and 30° for tetrahedral packing, with all the liquid bridges fusing together and eliminating the liquid bridge force. From Figs. 2 and 3, both

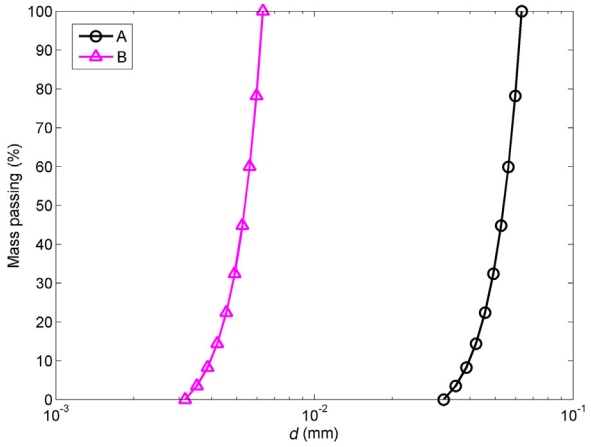

Fig. 4. Particle size distributions of narrow samples A (coarse) and B (fine).

the SWCC and SSCC exhibit a sudden transition from the pendular regime to a fully saturated state. All of the above phenomenological and quantitative behaviors agree well with the analytical solutions (Wang & Li, 2015a). This verifies the liquid bridge model and shows it is suitable for simulating the hydraulic response of unsaturated granular materials. The dramatic variation in suction and suction stress in Figs. 2 and 3 can be attributed to the simultaneous fusion of liquid bridges with growing water saturation.

SSCCs of various granular packings

SSCCs of differently sized packings

To model typical silt and clay soil systems, we generate the dispersive particle size distributions of a coarse sample labeled A and a fine sample labeled B, as shown in Fig. 4. We use suction loading tests to obtain the SSCCs of these two samples in Fig. 5. As suction approaches zero with increasing water content, suction stresses in both samples A and B vanish. In contrast, when air enters, the suction stress increases. The critical suctions for coarse sample A and fine sample B are about 3 kPa and 30 kPa, respectively, which agree well with typical air entry values for silt and clay (Lu et al., 2010). The maximal suction stresses of samples A and B are 5 kPa and 50 kPa, respectively. The typical cohesion of silt is 1–10 kPa, and that of clay is 30–65 kPa according to the Handbook of Engineering

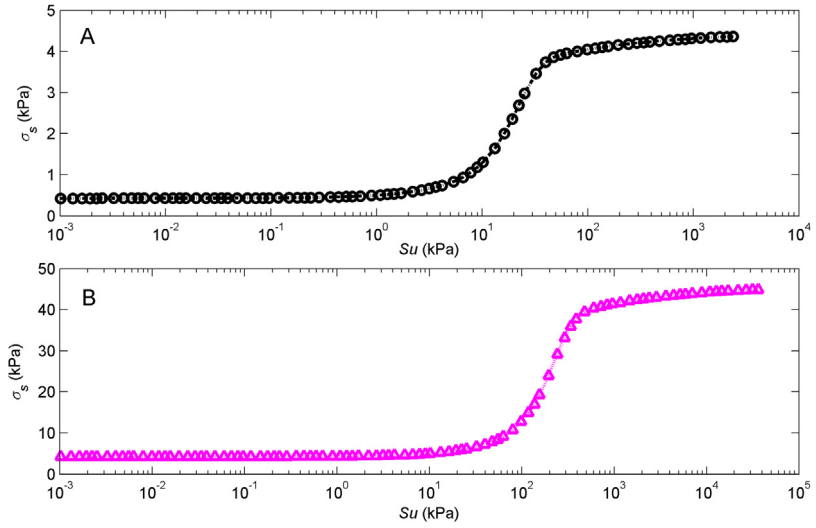

Fig. 5. SSCCs of narrow-sized granular packings A (coarse) and B (fine).

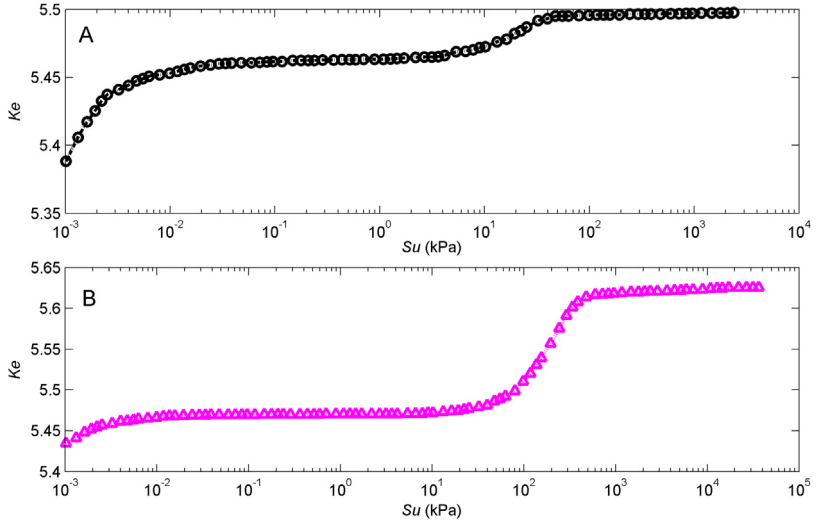

Fig. 6. Average liquid bridge number versus suction for narrow-sized packings A (coarse) and B (fine).

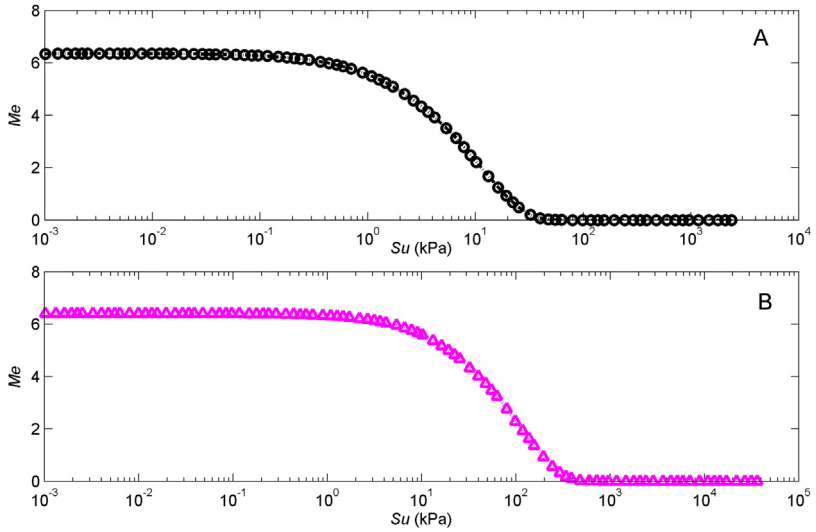

Fig. 7. Average fusion number evolution for narrow-sized granular packings A (coarse) and B (fine).

Geology (Chang & Zhang, 2007). Because the cohesion and suction stress have the same order of magnitude, there might be some relationship between them (Lu & Likos, 2004). Therefore, the concept of suction stress seems very helpful for establishing a strength theory for unsaturated granular materials.

Figs. 6 and 7 show the average number of liquid bridges per particle, *Ke*, and average fusion number per bridge, *Me*. The calculated value of *Ke* is about 5.5 for both coarse sample A and fine sample B, which implies the contact and liquid bridge pattern stays almost the same in the suction domain tested. From Fig. 7, the fusion number increases from zero at high suction to about 6 at low suction. This is the key mechanism for cohesion and suction stress variation. At high suction, the liquid bridges separate from each other, so the contribution of the liquid bridge force to the suction stress is high. At low suction, the liquid bridge force is reduced or even vanishes, causing a low suction stress. A mesoscale theory that includes microscopic information such as the contact network and liquid bridge pattern and macroscopic information such as the suction stress would be very helpful for understanding these phenomena in depth.

SSCCs of granular packings with different particle size distributions

Four samples are generated using four different PSDs (PSD1, PSD2, PSD3 and PSD4) as shown in Fig. 8, where the PSD is produced by a regularized incomplete beta function (Wang & Li, 2015b). PSD1 and PSD2 are narrow distributions, meaning more uniform, while PSD3 and PSD4 are more dispersive, the latter of which might correspond to a more realistic granular material. PSD1 and PSD4 hold more fine particles than PSD2 and PSD3. SSCCs for the four dispersive samples are calculated with the liquid bridge model and shown in Fig. 9. Compared with the SSCCs of the crystal packings in Figs. 2 and 3, the variations of the SSCCs of the dispersive granular samples appear more moderate in the whole suction domain. The suction stresses of the four samples are almost eliminated as the suction vanishes. At high suction, the suction stresses of the samples generated by PSD1 and PSD4 are obviously greater than those of the other two samples owing to the larger content of fine particles (about 40% smaller than 0.05 mm).

Figs. 10 and 11 show the evolution of the average liquid bridge number *Ke* and average fusion number *Me*. The average liquid bridge number for each particle is almost invariant in the whole suction domain studied because isotropic suction loading seems to

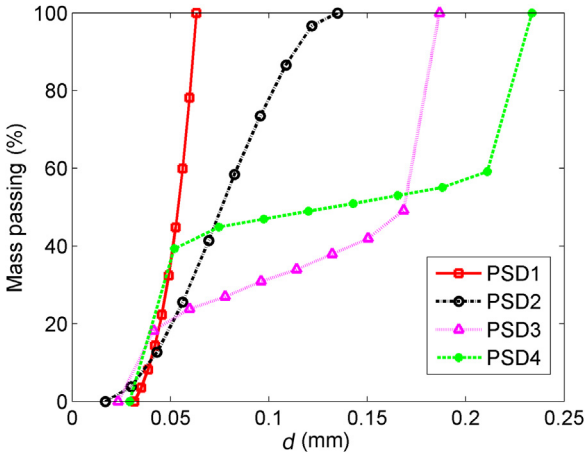

Fig. 8. Particle size distributions of four granular packings.

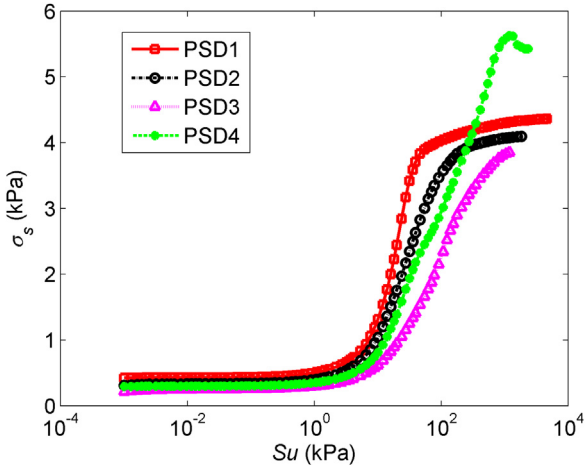

Fig. 9. SSCCs of four granular packings produced by the liquid bridge model.

play no role in forming a particle contact network. Because PSD1 and PSD4 have large liquid bridge numbers at high suction and higher fine particle content, their suction stresses at high suction are higher than those of PSD2 and PSD3. Fig. 11 shows that fusion number increases from zero in a pure separated state at high suc-

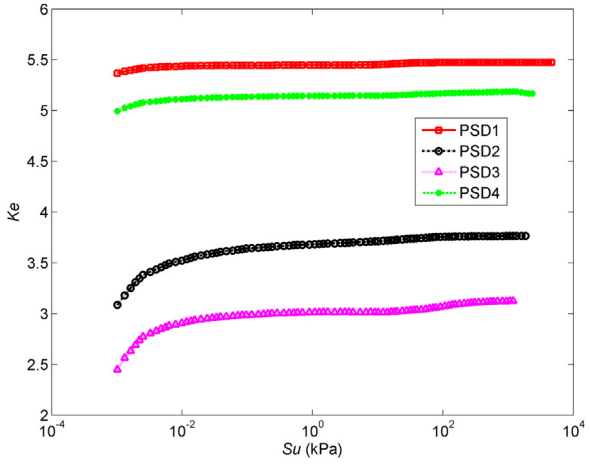

Fig. 10. Average liquid bridge number versus suction for four granular packings produced by the liquid bridge model.

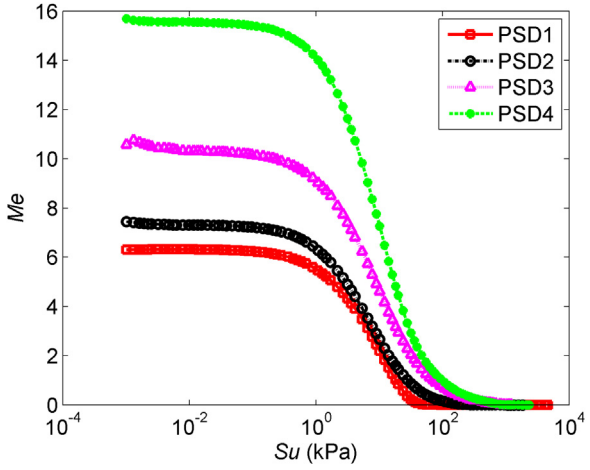

Fig. 11. Average fusion number versus suction for four granular packings produced by the liquid bridge model.

tion to a saturated value at low suction. Because the particle size distributions are more dispersive, the saturated fusion numbers of samples from PSD3 and PSD4 are larger than those of the other two PSDs. We may find that liquid bridge number is mainly controlled by fine particle content, while fusion number depends on PSD dispersion. Fine particle content, liquid bridge distribution, particle size and fusion distribution are key determinants of the macroscopic SSCC behavior. However, it is still challenging to establish such a theory for granular packing or even an empirical formula for SSCC.

A new SSCC model

With the aforementioned calculation and analysis, suction stress as a material response may be treated as a state variable like pressure, while suction is regarded as an external load. For this purpose, section 4 is devoted to a new SSCC model and its applications.

Model description

As suction stress is caused by suction, an SSCC should be formulated as a constitutive law for unsaturated granular materials in a way similar to the SWCC and HCF. The expression of an SSCC quantitatively links the hydraulic response and deformation. Previous methods for coupling seepage and deformation included Bishop's effective stress concept and two-variable theory. Bishop's effective stress has an undetermined parameter χ, whereas two-variable theory needs multiple experiments to find numerous constants. Lu et al. have formulated a simple thermodynamic SSCC model, but it ignores the capillary effect in the funicular and pendular regimes (Lu et al., 2010). Therefore, a new SSCC formula is needed.

Table 1
SSCC model data for the six DEM samples.

Item	A	B	PSD1	PSD2	PSD3	PSD4
a	3.5	3.3	3.5	15	15	5
b (kPa^{-1})	0.222	0.022	0.222	0.25	0.175	0.238

Lu's SSCC model only applies in the capillary regime where saturation is high (low suction). Although the theory is based on free energy, it is difficult to apply to low saturation such as the pendular or funicular regimes. Furthermore, Lu's SSCC model finally recovers the same form as Bishop's effective stress framework using $\chi = Sr$. As long as the SSCC constitutes responses between suction stress and external load suction, neither the two-variable framework nor effective stress framework is needed. Meanwhile, it is difficult to derive an SSCC from liquid bridge number, fusion number and contact network using only mesoscale analysis. An alternative is DEM analysis. The numerical results in Figs. 2(b), 3 (b), show that an SSCC has two common features: it approaches zero at low suction and approaches a saturated value at high suction. Consequently, we propose the following two-parameter hyperbolic model for an SSCC:

$$\sigma_s = \frac{Su}{a + bSu}, \tag{5}$$

which has only two parameters, a and b. Compared with parameter χ in Bishop's effective stress and tan ϕ^b in extended Mohr–Coulomb strength theory, a and b in Eq. (5) have obvious physical meanings: $1/a$ is the SSCC slope at the origin, and $1/b$ denotes the saturated suction stress at very high suction. Both a and b are easily determined via data fitting. Eq. (5) is termed the new SSCC model and is applied to various cases below.

Analysis of DEM simulation

Using the model in Eq. (5), data fitting is implemented as shown in Table 1 for all of the SSCCs in Figs. 5 and 9. The SSCC model predictions in Figs. 12 and 13 agree well with the DEM simulation for all the six cases for values close to zero at low suction and an almost saturated value at high suction. However, at low suction, the model prediction is even closer to zero than the DEM prediction because the cohesive force in the liquid bridge model in Eq. (2) does not fully decrease to zero, which might result in a small suction stress through the volume average in Eq. (4). In real situations, suction stress vanishes quickly because most of the pores are filled with water at saturation. Therefore, the new SSCC model reflects suction stress behavior for suction from 0 to 10^5–10^6 kPa. However, there are still some deviations in the transition region.

Application to real soil

We use four samples of real unsaturated granular materials from the literature to examine the validity of the new SSCC model. They are sand clay (Blight, 1967), Madrid clay sand (Escario & Saze, 1986), Jossigny silt (Cui & Delage, 1993) and kaolin (Khalili & Khabbaz, 1998). The fitted data are listed in Table 2. Fig. 14 shows the predicted SSCCs for the four granular materials. For limited data in a limited suction range, the predictions of the proposed SSCC model agree well with experiment. Furthermore, the proposed

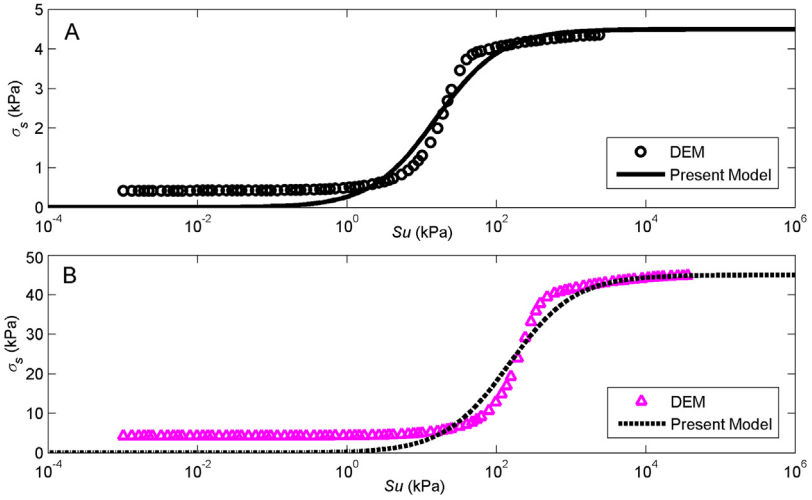

Fig. 12. SSCC model prediction for samples A (coarse) and B (fine).

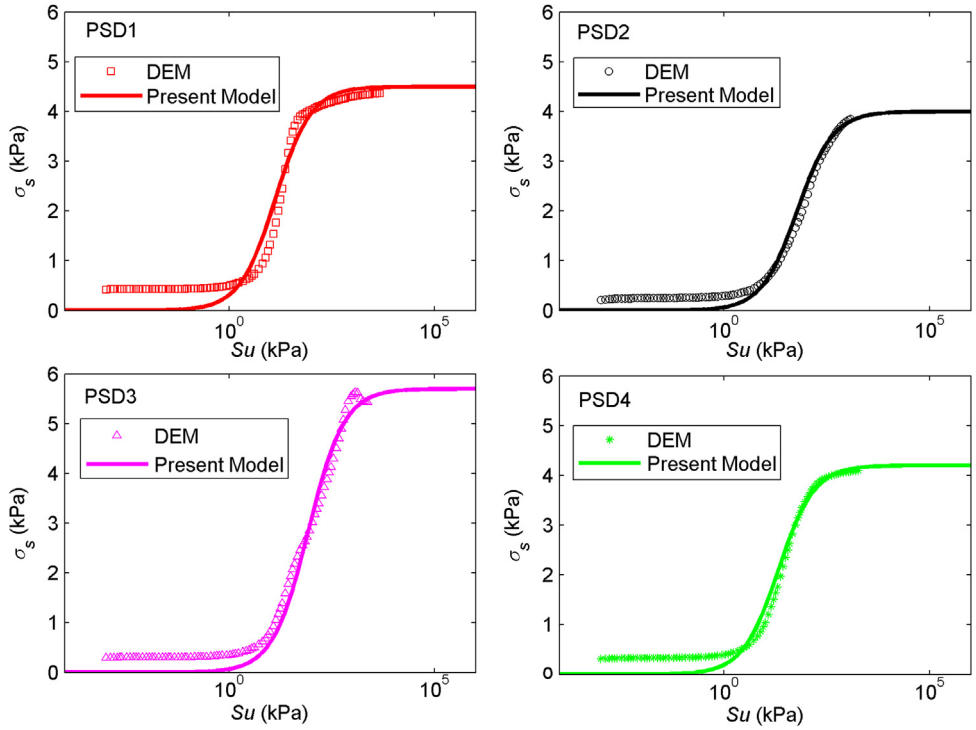

Fig. 13. SSCC model predictions for the samples generated by PSD1, PSD2, PSD3 and PSD4.

SSCC model coincides with Terzaghi's classical effective stress theory in a very narrow range close to saturation at low suction.

Effective stress and strength

Examination of Bishop's effective stress

In one-variable unsaturated granular material theory, Bishop's effective stress is widely used to link seepage and deformation. Bishop's effective stress formula reads

$$\sigma' = (\sigma - u_a) + \chi(u_a - u_w), \tag{6}$$

where σ', $(\sigma - u_a)$ and $(u_a - u_w)$ are the effective stress, net stress and suction, respectively. We note that the suction $(u_a - u_w)$ in Eq. (6) is the suction Su in Eq. (5). Here we use $(u_a - u_w)$ in all the strength theory following the convention in unsaturated soil engineering (Fredlund et al., 1993).

Table 2
SSCC model data for four real soils from the literature.

Item	Sand Clay	Clay Sand	Jossigny Silt	Kaolin
a	1.0	1.0	1.0	1.0
b (10^{-3} kPa^{-1})	8.33	2.94	1.61	0.25

The parameter $0 \le \chi \le 1.0$ is used to connect the totally saturated and totally dry regimes. Determining χ is different from case to case. In Figs. 15 and 16, we examine the DEM simulated results in Figs. 5 and 9 using the empirical formulae $\chi = Sr$, which we call Theory 1, and $\chi = Sr^3$, which we call Theory 2. The term Sr is the saturation (water content) that fulfills the requirement $0 \le \chi \le 1.0$ (Lewis & Schrefler, 1998). Theory 1 is widely used nowadays and

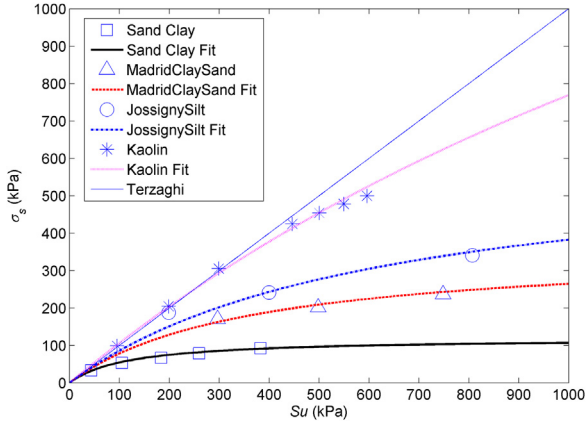

Fig. 14. SSCC model predictions for four real soils and Terzaghi's effective stress.

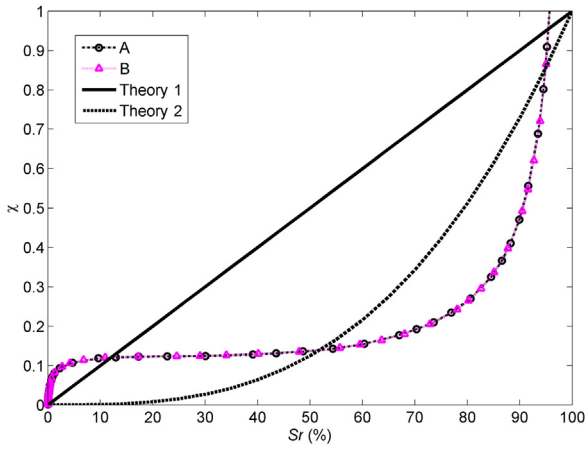

Fig. 15. χ Parameter in Bishop's effective stress and DEM results for samples A and B. $\chi = Sr$ for Theory 1 and $\chi = Sr^3$ for Theory 2, where Sr is saturation.

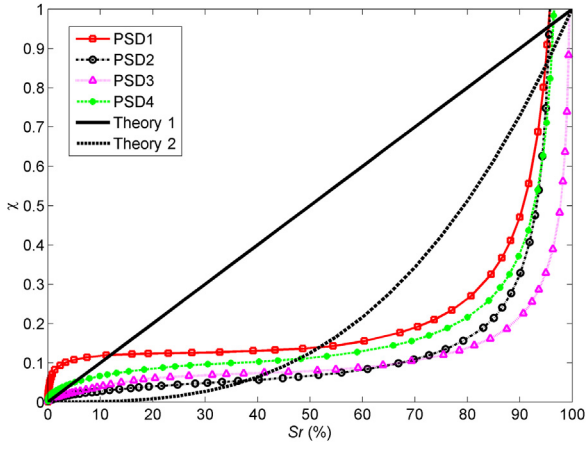

Fig. 16. χ Parameter in Bishop's effective stress and DEM results for samples PSD1, PSD2, PSD3 and PSD4. $\chi = Sr$ for Theory 1 and $\chi = Sr^3$ for Theory 2, where Sr is saturation.

is also in the commercial software Abaqus (Anon., 2016). However, Theory 1 and Theory 2 deviate a lot from DEM results. Theory 2 seems a bit better than Theory 1 at least for the suction domain covered by the DEM results. Application to real soils requires data fitting for χ, but no result has been found, which means this theory cannot be used for stress decomposition in unsaturated granular materials. In contrast, the suction stress proposed by Lu and Likos (2006) and mesoscale analytical method in this study are physically

Table 3
Strength model data for three real soils from the literature.

Item	Glacial Till	Red Silt	Madrid Clay
c' (kPa)	10	30	49
ϕ' (°)	25.5	31	38.4
a	1.0	1.0	1.0
b (10^{-3} kPa^{-1})	1.67	1.11	1.92

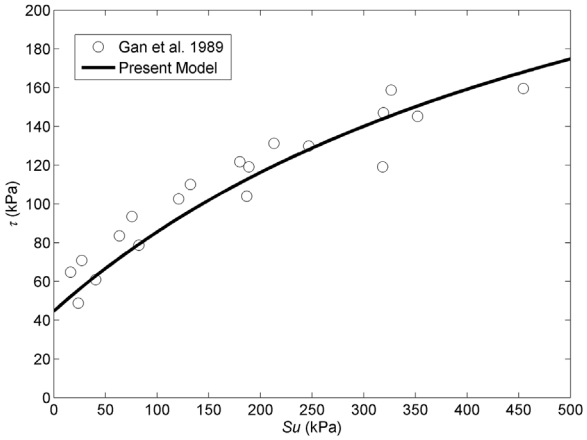

Fig. 17. Strength of compact glacial till predicted by SSCC-based theory.

robust. The proposed SSCC model in Eq. (5) is similar to the SWCC and HCF and has upgraded the framework of unsaturated granular materials to some extent.

Strength theory based on SSCC

Another important issue in geotechnical engineering is how to estimate material strength, which thus far has not been resolved for unsaturated granular materials. Lu's suction stress concept has shed light on its resolution (Lu et al., 2010). Many experiments have demonstrated that strength varies nonlinearly with suction, which cannot be explained by classical strength theory such as extended Mohr–Coulomb theory (Fredlund et al., 1993) in Eq. (7). Eq. (7) can only be considered a reformulation of Bishop's effective stress. The frictional angle ϕ^b associated with suction is obtained by numerical fitting when plotted versus saturation or suction. In real engineering applications, values found for ϕ^b are either not constant or even physically unreasonable. Similar circumstances arise in handling the parameter χ for Bishop's effective stress theory

$$\tau = c' + (\sigma - u_a)\tan\phi' + (u_a - u_w)\tan\phi^b, \quad (7)$$

where τ is the strength, $(u_a - u_w)$ the suction, c' the cohesion and ϕ' the frictional angle.

The new strength formula in terms of suction stress for unsaturated granular material is

$$\tau = c' + [(\sigma - u_a) + \sigma_s]\tan\phi', \quad (8)$$

Where c' and ϕ' are the cohesion and friction angle in a saturated state, respectively, and σ_s is the suction stress in Eq. (5) for the SSCC model. c', ϕ' and σ_s are well defined physical variables. Three literature examples are used to examine the present strength formula on the basis of suction stress in the proposed SSCC model. The compact glacial till data are from Gan et al. (1988), and the red silt and Madrid clay data are from Escario (1989). SSCC data for the three examples are fitted as shown in Table 3, while c' and ϕ' are directly acquired from the literature.

The predicted curves of strength versus suction are shown in Fig. 17 for compact glacial till and in Fig. 18 for red silt and Madrid clay. The strength-versus-suction curves in Figs. 17 and 18

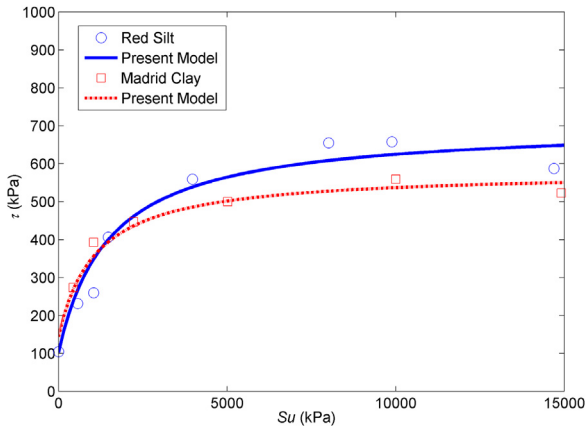

Fig. 18. Strength of red silt and Madrid clay predicted by SSCC-based theory.

agree well with experiment. The results exhibit not only the same variational trend but also the increase in strength with suction. For instance, the variation of strength versus suction for compact glacial till in Fig. 17 is moderate. In contrast, the variation for red silt and Madrid clay in Fig. 18 is drastic and nonlinear for suction between 0 and 500 kPa. This is beyond the capability of extended Mohr–Coulomb theory.

Conclusions

We proposed an approach for deriving the SSCCs of unsaturated granular materials based on the liquid bridge model and DEM simulation. It was verified through a series of parallel simulations and comparisons with theoretical results for various granular packings of different particle size distributions, including cubic and tetrahedral crystal packing. Later, a new SSCC model with two parameters was proposed and used to predict stress and strength behavior in various situations. The main achievements and conclusions of this study are:

(1) The SSCCs of granular materials were generated for the first time. We used a mesoscale liquid bridge model and DEM simulation to obtain the SSCCs for unsaturated granular materials with crystal and dispersive particle packing, which is an effective approach for understanding both macroscopic phenomena and microscopic mechanisms of unsaturated granular materials.
(2) We proposed a new SSCC model with two physically defined parameters, and used it to predict the SSCCs of both DEM cases and real granular materials. The agreement between the formula and simulation or experiment is satisfactory.
(3) A strength expression for unsaturated granular materials was presented that is based on the new SSCC model. This equation successfully predicts the nonlinear variation of strength versus suction and overcomes the weaknesses of both Bishop's effective stress and extended Mohr–Coulomb strength theory.
(4) After being further developed to the level of the SWCC and HCF, the SSCC can become a commonly used law for unsaturated granular materials to determine the coupling between hydraulic behavior and deformation response. With Lu's suction stress concept and the new SSCC model, a new theoretical framework for unsaturated granular materials can emerge in the future.

Meanwhile, questions such as deriving an SSCC directly from liquid bridge information and the microscopic contact network are still open for resolution.

Conflict of interests

The authors declare that they have no known competing financial interests or personal relationships that could have appeared to influence the work reported in this paper.

Acknowledgements

This work was supported by the National Natural Science Foundation of China (Grant Nos. 12032005, and 11602278), Beijing Institute of Technology Research Fund Program for Young Scholars, and National Key R&D Program of China (Grant No. 2018YFC1505504).

References

Alonso, E. E., Gens, A., & Josa, A. (1990). A constitutive model for partially saturated soils. *Géotechnique*, *40*(3), 405–430. http://dx.doi.org/10.1680/geot.1990.40.3.405
Anon. (2016). *Abaqus analysis user's manual, Version 2016. Chapter 6.8 Coupled pore fluid flow and stress analysis*. Providence, RI, USA: Dassault Systemes.
Belheine, N., Plasslard, J. P., Donze, F. V., Darve, F., & Seridi, A. (2009). Numerical simulation of drained triaxial test using 3d discrete element modeling. *Computers and Geotechnics*, *36*(1–2), 320–331. http://dx.doi.org/10.1016/j.compgeo.2008.02.003
Biot, M. A. (1941). General theory of three-dimensional consolidation. *Journal of Applied Physics*, *12*(2), 155–164. http://dx.doi.org/10.1063/1.1712886
Bishop, A. W. (1959). The principle of effective stress. *Teknisk ukeblad*, *39*, 859–863.
Blight, G. E. (1967). Effective stress evaluation for unsaturated soils. *Journal of Soil Mechanics and Foundations*, *93*(2), 125–148. http://dx.doi.org/10.1016/0022-4898(67)90056-0
Caulk, R., Sholtès, L., Krzaczek, M., & Chareyre, B. (2020). A pore-scale thermos-hydro-mechanical model for particulate systems. *Computer Methods in Applied Mechanics and Engineering*, *372*, 113292. http://dx.doi.org/10.1016/j.cma.2020.113292
Chang, S. P., & Zhang, S. M. (2007). *Handbook of engineering geology*. Beijing: China Architecture & Building Press (Chapter 1 of Part 3).
Cui, Y. J., & Delage, P. (1993). On the elasto-plastic behavior of an unsaturated silt. *Unsaturated Soils, ASCE*, *39*, 115–126.
Cundall, P. A., & Strack, O. D. L. (1979). A discrete numerical model for granular assemblies. *Geotechnique*, *29*(1), 47–65. http://dx.doi.org/10.1680/geot.1979.29.1.47
Escario, V. (1989). Strength and deformation of partly saturated soils. In *Proceedings of the 12th International Conference on Soil Mechanics and Foundation Engineering* (pp. 43–46).
Escario, V., & Saze, J. (1986). The shear strength of partly saturated soils. *Geotechnique*, *36*(3), 453–456. http://dx.doi.org/10.1680/geot.1986.36.3.453
Fredlund, D. G., Rahardjo, H., & Rahardjo, H. (1993). *Soil mechanics for unsaturated soils*. New York: John Wiley & Sons (Chapter 1, 3 & 9).
Gan, J. K. M., Fredlund, D. G., & Rahardjo, H. (1988). Determination of the shear strength parameters of an unsaturated soil using the direct shear test. *Canadian Geotechnical Journal*, *25*(3), 500–510. http://dx.doi.org/10.1139/t88-055
Khalili, N., & Khabbaz, M. H. (1998). A unique relationship of chi for the determination of the shear strength of unsaturated soils. *Geotechnique*, *48*(5), 681–687. http://dx.doi.org/10.1680/geot.52.1.76.40832
Lewis, R. W., & Schrefler, B. A. (1998). *The finite element method in the static and dynamic deformation and consolidation of porous media* (2nd ed.). Chichester: John Wiley & Sons (Chapter 4).
Lu, N. (2008). Is matric suction a stress variable? *Journal of Geotechnical and Geoenvironmental Engineering*, *134*(7), 899–905. http://dx.doi.org/10.1061/(asce)1090-0241(2008)134:7(899)
Lu, N., & Likos, W. J. (2004). *Unsaturated soil mechanics*. New Jersey: Wiley (Chapter 6 &9).
Lu, N., & Likos, W. J. (2006). Suction stress characteristic curve for unsaturated soil. *Journal of Geotechnical and Geoenvironmental Engineering*, *132*(2), 131–142. http://dx.doi.org/10.1061/(asce)1090-0241(2006)132:2(131)
Lu, N., Godt, J. W., & Wu, D. T. (2010). A closed-form equation for effective stress in unsaturated soil. *Water Resource Research*, *46*(5) http://dx.doi.org/10.1029/2009wr008646. W05515
Scholtès, L., Chareyre, B., Nicot, F., & Darve, F. (2009). Micromechanics of granular materials with capillary effects. *International Journal of Engineering Science*, *47*(1), 64–75. http://dx.doi.org/10.1016/j.ijengsci.2009.10.003
Terzaghi, K. (1925). Principles of soil mechanics, IV—Settlement and consolidation of clay. *Engineering News-Record*, *95*(3), 874–878.

Wang, X., & Li, J. (2014). Simulation of triaxial response of granular materials by modified DEM. *Science China Physics Mechanics & Astronomy*, *57*(12), 2297–2308. http://dx.doi.org/10.1007/s11433-014-5605-z

Wang, X., & Li, J. (2015a). A novel liquid bridge model for estimating SWCC and permeability of granular material. *Powder Technology*, *275*, 121–130. http://dx.doi.org/10.1016/j.powtec.2015.01.044

Wang, X., & Li, J. (2015b). Influence of particle gradation curve on granular packing characteristics. *Procedia Engineering*, *102*, 1827–1834. http://dx.doi.org/10.1016/j.proeng.2015.01.320

Wang, X. L., Zhang, Z., & Li, J. C. (2019). Triaxial behavior of granular material under complex loading path by a new numerical true triaxial engine. *Advanced Powder Technology*, *30*, 700–706. http://dx.doi.org/10.1016/j.apt.2018.12.020

Yuan, C., & Chareyre, B. (2017). A pore-scale method for hydromechanical coupling in deformable granular media. *Computer Methods in Applied Mechanics and Engineering*, *318*, 1066–1079. http://dx.doi.org/10.1016/j.cma.2017.02.024